In–situ modification of UiO–66(Zr) organic ligand to synthesize highly recyclable solid acid for biodiesel production

Li, Hui; Wang, Tianyu; Chu, Huijun; Rokhum, Samuel Lalthazuala; Zhang, Yaning; Yu, Hewei; Xiao, Qiangqiang; Guo, Min; Ma, Xiaoling; Li, Shijie; Li, Guoning

DOI:
10.1016/j.cherd.2024.04.040

Chemical Engineering Research and Design 205 (2024) 713–721

Contents lists available at ScienceDirect

Chemical Engineering Research and Design

journal homepage: www.elsevier.com/locate/cherd

In–situ modification of UiO–66(Zr) organic ligand to synthesize highly recyclable solid acid for biodiesel production

Hui Li [a], Tianyu Wang [a], Huijun Chu [a], Samuel Lalthazuala Rokhum [b], Yaning Zhang [c], Hewei Yu [d], Qiangqiang Xiao [a], Min Guo [a], Xiaoling Ma [e,*], Shijie Li [a], Guoning Li [a,*]

[a] School of Thermal Engineering, Shandong Jianzhu University, Jinan 250101, PR China
[b] Department of Chemistry, National Institute of Technology Silchar, Assam 788010, India
[c] School of Energy Science and Engineering, Harbin Institute of Technology (HIT), Harbin 150001, PR China
[d] School of Energy and Power Engineering, Qilu University of Technology (Shandong Academy of Sciences), Jinan 250353, PR China
[e] Birmingham Centre for Energy Storage, School of Chemical Engineering, University of Birmingham, Birmingham B15 2TT, UK

ARTICLE INFO

Keywords:
Biodiesel
UiO–66(Zr)
In–situ modification
Sulfonic acid group

ABSTRACT

To transfer high free fatty acid oil into biodiesel in mild conditions is still facing challenge, thereinto, the key is efficient acid catalyst. In this study, 2,5–dimercaptoterephthalic acid was adopted to substitute terephthalic acid as ligand for UiO–66–$(SH)_2$ synthesis, then the sulfydryl (–SH) was in-situ oxidized by hydrogen peroxide and acidified via sulfuric acid thus generating sulfonic catalyst UiO–66–$(SO_3H)_2$. To further reveal the relationship between physico–chemical property and catalytic activity, catalyst was characterized via thermogravimetry analysis (TG), X–ray diffraction (XRD), N_2 absorption–desorption, scanning electron microscope (SEM), Fourier transform infrared spectroscopy (FTIR), and pyridine absorption–Fourier transform infrared spectroscopy (Py–FTIR). Results indicate the in–situ modification increases the quantity of acid sites for UiO–66(Zr), where the acidity is aggrandized from 0.02 mmol/g to 2.28 mmol/g. The maximum conversion of oleic acid to biodiesel was 86.52 % with catalyst amount of 10 wt% and molar ratio of methanol/oleic acid of 15 at 90 °C within 4 h. Moreover, UiO–66–$(SO_3H)_2$ exhibited favorable reusability and water resistance, which maintained an excellent esterification conversion after four cycles and no obvious impact was detected as the water content was 10 wt%. The quality of obtained biodiesel in this study satisfied the European Union standard of EN 14214, which could be used as transport fuel.

1. Introduction

With the growing fossil energy shortage and environmental crisis aroused by fossil energy consumption, it is crucial to develop green energy resources. Biodiesel, composed of fatty acid methyl esters (FAME), is considered as an ideal substitute for fossil oil owing to its excellent combustion performance, environment friendly, and renewability (Zeppini and van den Bergh, 2020; Zhou et al., 2022). Normally, biodiesel is produced via transesterification of refined oils such as animal and plant oils with methanol. However, the refined oils account for 75 % of biodiesel production cost, thus restricting its popularization and application (Xie and Wan, 2019). While, massive low–cost feedstock, like waste cooking oils (WCOs) and gutter oil, are not effectively utilized in China, which is expected as an ideal feedstock oil for biodiesel production. The traditional basic catalysts (NaOH and KOH) used in transesterification are not applicable for WCOs and gutter oil, due to the intrinsic higher water content and free fatty acid (FFA) would lead to hydrolysis and saponification.

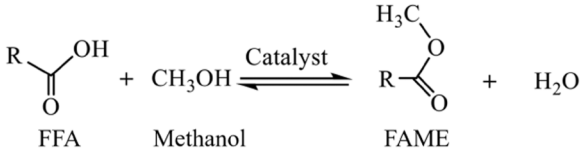

By contrast, acid catalyst could address the above demerits of basic catalyst and achieve the esterification by transforming FFA into biodiesel (**Eq. 1**) (Alvear-Daza et al., 2021). Thereinto, heterogeneous acids have been gained extensive attention like carbon–based solid acid (Alvear-Daza et al., 2021), zeolite molecular sieves (Prinsen et al.,

* Corresponding authors.
E-mail addresses: x.ma.2@bham.ac.uk (X. Ma), liguoning20@sdjzu.edu.cn (G. Li).

https://doi.org/10.1016/j.cherd.2024.04.040
Received 21 February 2024; Received in revised form 10 April 2024; Accepted 19 April 2024
Available online 22 April 2024

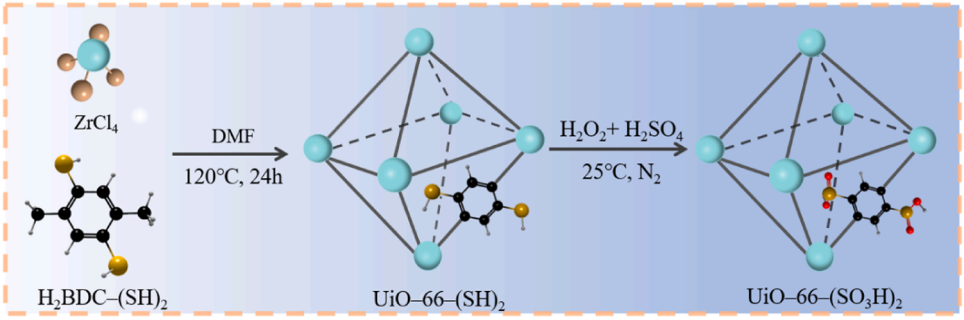

Fig. 1. Preparation process of UiO–66–$(SO_3H)_2$.

2018), sulfated metal oxides (da Silva and Rodrigues, 2020), heteropoly acid (Ning et al., 2020), etc. Although heterogeneous acids exhibit high catalytic activity, they suffer from the reusability issues due to active site leaching (Rahmani Vahid et al., 2018; Wang et al., 2020), besides, the poor pore structure aggravates this drawback (Qi et al., 2016).

Metal organic frameworks (MOFs) are crystal materials of periodic multi–dimensional pore structures composed of metal centers and organic ligands (Wang et al., 2024). In light of the spectacular high surface area, pore volume, and highly ordered topological structure (Liu et al., 2019; Zheng et al., 2018), MOFs are widely used in adsorption (Gaikwad et al., 2022; Yıldız and Erucar, 2022), photocatalysis (Qiu et al., 2022; Xia et al., 2021), catalysis (Li et al., 2021c; Lu et al., 2022), and so on. Moreover, MOFs can be modified through post–synthesis and in–situ modification method to obtain the specific morphological, controlled pores, and surface functionality. Zhang et al. (2023) prepared the Bi-based MOFs and used to impregnate the phosphomolybdic acid (PMA@Bi-BTC) for catalyzing esterification of oleic acid and methanol. With the optimum conditions, the conversion of 92.5 % was achieved with molar ratio of methanol to oleic acid of 20:1 and 0.15 g catalyst at 160 °C in 3 h. Ruatpuia et al. (2023) achieved an efficient CaO/ZnO catalyst through ZIF-8, it exhibits promising catalytic performance in transesterification, in which the molar ratio of methanol to soybean oil was 20:1 with 7 wt% catalyst amounts at 90°C for 50 min, resulting in 97.4 % biodiesel yield. Cong et al. (2023) constructed a magnetic catalyst of Na_2SiO_3/Ni-MOF, by assisted with microwave heating, a desirable biodiesel yield of 95.3 % was obtained with catalyst dosage of 9 wt% and molar ratio of methanol to waste oil of 15:1 at 90 °C in 15 min.

In most cases, post–synthesis modification is employed to synthesize acid catalyst. For instance, Li et al. (2021c) adopted MIL-100(Fe) to support ammonium sulfate ($(NH_4)_2SO_4$) for solid acid preparation. The synthesized catalyst exhibited favorable catalytic activity of 90.95 % with molar ratio of methanol/oleic acid of 8:1, catalyst amount of 8 wt% at 70 °C for 2 h. Lu et al. (2022) grafted acidic ionic liquid into NH_2-UiO-66, the obtained catalyst achieved the esterification conversion of 95.22 % with molar ratio of methanol/oleic acid of 14:1, catalyst amount of 5 wt% at 75 °C for 6 h. The homogeneity of active site distribution obtained from post–synthesis modification is unsatisfactory. Furthermore, high temperature treatment is normally required to achieve the active site and strengthen the connection between support and active site. Therefore, it is imperative to achieve a uniform dispersion of active site on MOF. Inspired by the periodic arrangement of metal ion and organic ligand, if the organic ligand could be modified with active site, it could achieve the uniform distribution of active site.

UiO–66(Zr) is a representative MOFs, which is composed of $[Zr_6O_4(OH)_4(R–CO_2)_{12}]$ metal cluster and 12–coordinated to terephthalic acid (Jrad et al., 2021; Wu et al., 2022). This dense coordination makes the whole structure stably connected. According to the reported literature (Valenzano et al., 2011), UiO–66(Zr) is fairly stable as temperature is up to 500 °C, even though in a wide range of chemical solutions. Nonetheless, UiO-66(Zr) exhibits non-catalytic activity for esterification due to weak acid sites. To address this, Rokhum Group functionalized UiO-66(Zr) by using defect site coordination strategy, where UiO-66(Zr) was mixed with acid reagent, such as sulfamic acid and chlorosulfonic acid, the obtained catalyst exhibited outstanding catalytic activity in biodiesel production (Gouda et al., 2022; Gouda et al., 2024).

The advantage of MOFs is functional tunability, wherein the functional group can be in-situ tailored and modified. Inspired by this, 2,5–dimercaptoterephthalic acid ($H_2BDC–(SH)_2$) is adopted as organic ligand to substitute the terephthalic acid (H_2BDC) for UiO–66–$(SH)_2$ synthesis, then the sulfhydryl group (–SH) is oxidized with hydrogen peroxide and acidified with sulfuric acid into sulfonic group ($–SO_3H$) to obtain solid acid. In detail, H_2O_2 amount and oxidation time are concerned to optimize the synthesis conditions. Furthermore, catalyst is characterized via X–ray diffraction (XRD), thermogravimetric analysis (TG), N_2 adsorption/desorption, scanning electron microscope (SEM), Fourier transform infrared spectroscopy (FTIR), and Fourier transform infrared spectroscopy of pyridine adsorption (py–FTIR). In addition, the influence of esterification parameters including catalyst amount, molar ratio of methanol/oleic acid, reaction time, and reaction temperature on conversion are evaluated via single factor method. Ultimately, the reusability and water resistance of UiO–66–$(SO_3H)_2$ are further assessed.

2. Materials and methods

2.1. Materials

Analytical reagents of zirconium tetrachloride ($ZrCl_4$), acetic acid, terephthalic acid, 2,5–dimercaptoterephthalic acid, N, N–dimethylformamide (DMF), methanol (CH_3OH), hydrogen peroxide (H_2O_2), sulfuric acid (H_2SO_4), ethanol (CH_3CH_2OH), and oleic acid ($C_{17}H_{33}COOH$) are directly used in catalyst preparation without further treatment.

2.2. Catalyst preparation

2.2.1. UiO–66–$(SH)_2$ synthesis

0.227 mmol $ZrCl_4$ and 0.227 mmol $H_2BDC–(SH)_2$ are mixed with 34 mmol DMF and stirred at 50 °C for 30 min. Afterwards, 11.35 mmol acetic acid is added to the above mixtures, and then placed in a teflon–lined stainless steel autoclave reactor at 120 °C for 24 h. With that, the obtained solid is washed three times in DMF and methanol, respectively, then it is dried at 100 °C for 8 h and eventually dried vacuum at 100 °C for 5 h labeled as UiO–66–$(SH)_2$.

2.2.2. UiO–66–$(SO_3H)_2$ preparation

0.2 g UiO–66–$(SH)_2$ is blended with 10 mL methanol in a flask sealed with nitrogen. Next, 20 mL H_2O_2 (concentration 30 wt%) is added into flask to oxidize –SH group and further protonated with 20 mL H_2SO_4 (0.1 mol/L) for 1 h. The solid is isolated via centrifugation and rinsed

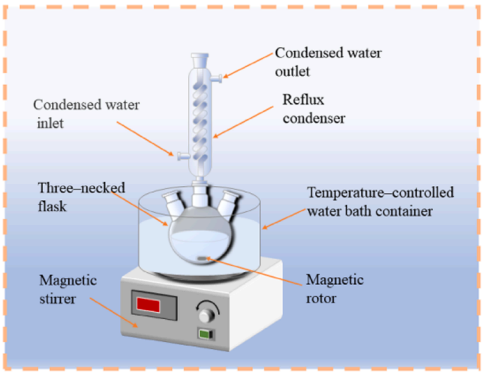

Fig. 2. Schematic diagram of the instrument of oleic acid esterification.

with deionized water until the filtrate is neutral. After that, the rinsed solid is dried at 100 °C for 12 h, and then transferred to a vacuum drying oven at 100 °C for 6 h resulting in catalyst of UiO–66–$(SO_3H)_2$ as show in Fig. 1.

2.3. Catalyst characterizations

Thermal property of catalyst is evaluated by using TGA/DSC3+ thermal gravimetric analyzer (Mettler Toledo Co., Ltd, Switzerland), in which the temperature is linearly increased from 30 °C to 800 °C with heating rate of 20 °C/min under nitrogen atmosphere. Crystalline phase is operated on SmartLab X ray diffractometer (Rigaku Co. Ltd., Japan), the diffraction pattern is recorded from 5° to 90° with voltage of 40 kV and 40 mA. To measure catalyst surface area and pore volume, catalyst is degassed at 150 °C for 8 h before the test and nitrogen absorption/desorption is conducted in Belsorp–Max (Microtrac Inc Co., Ltd., Japan) at –198 °C. The catalyst morphology is taken via ZEISS SUPRA 55 field emission scanning electron microscope (Carl Zeiss, Co., Ltd, Germany). The acid site property of catalyst is evaluated via py-FTIR, wherein the catalyst firstly absorbs pyridine and then desorbs at 70 °C, 200 °C, and 350 °C, the FTIR spectrum is obtained from 1200 cm^{-1} to 2600 cm^{-1} through Nicolet 6700 FTIR spectrometer (Thermo Nicolet Co., Ltd, USA). To evaluate the acidity, catalyst is mixed with 0.05 mol/L sodium chloride solution, then 0.05 mol/L NaOH is adopted to neutralize the mixture, in which phenolphthalein is used as an indicator. The consumed NaOH amount is acidity. Surface functional group is measured via Tensor 27 Fourier transform infrared spectrometer (Bruker Co., Ltd, Germany), the FTIR spectrum is recorded with wavelength range of 500–4000 cm^{-1} at room temperature.

2.4. Catalytic performance

Catalytic activity is examined by esterification of oleic acid and methanol, the esterification conversion (%) is adopted to describe catalytic performance determined by Eq. (2). Typically, a certain amount of oleic acid and methanol are blended in a three–neck flask connected with condenser tube, which is magnetically stirred until reaching the preset temperature (Fig. 2). Then, the prepared catalyst is added to the reactants and stirred for a certain time. After that, catalyst is separated via centrifugation and the upper layer is biodiesel. During this process, esterification parameters of catalyst amount (δ), molar ratio of methanol/oleic acid (ζ), reaction temperature (φ), and reaction time (τ) are studied.

$$Conversion = \frac{AV_i - AV_f}{AV_i} \times 100\% \quad (2)$$

Where AV_i and AV_f is the initial and final acid value of oleic acid, mg KOH/g.

2.5. Catalyst reusability and water resistance

Catalyst reusability is evaluated via consecutive batch experiment with optimal esterification parameters, where the catalyst is isolated via centrifugation and used directly to catalyze fresh oleic acid and methanol without further treatment. The water resistance is tested by adding a certain amount of water into oleic acid, the conversion variation is recorded to signify the ability of water resistance.

3. Results and discussion

3.1. Influence of H_2O_2 amount and oxidation time on catalytic activity

Hydrogen peroxide (H_2O_2) is essential for –SH transforming into $–SO_3H$, as a result, the strong Brønsted acid sites are introduced into the organic ligand (Andreoli, 1993). Influence of H_2O_2 amount, which is defined as H_2O_2 volume required to oxidize per gram of UiO–66–$(SH)_2$, and oxidation time (h) on catalytic activity are explored to optimize the synthesis factors. The esterification of oleic acid and methanol is progressed with catalyst amount of 10 wt%, molar ratio of methanol/oleic acid of 15 at 70 °C for 4 h.

As shown in Fig. 3**(a)**, H_2O_2 amount exerts impact on catalytic activity, where the conversion is gradually increased from 70.94 % to 82.28 % with aggrandizing H_2O_2 amount from 30 mL H_2O_2/g to 100 mL H_2O_2/g. While the conversion is tardily decreased to 81.18 % as H_2O_2 amount is further increased. –SH would be transformed into disulfide (–S═S–) rather than $–SO_3H$ when H_2O_2 amount is inadequate (Udenigwe et al., 2016), thus leading to the insufficient acquisition of $–SO_3H$. With regard to this, –SH is gradually oxidized into $–SO_3H$ with increasing H_2O_2 amount, wherein the maximum acidity of 2.28 mmol/L is obtained with 100 mL H_2O_2/g. Afterwards, the acidity is decreased as H_2O_2 amount exceeds 150 mL H_2O_2/g indicating the oxidation equilibrium point is achieved with 100 mL H_2O_2/g. Hence, the H_2O_2 amount

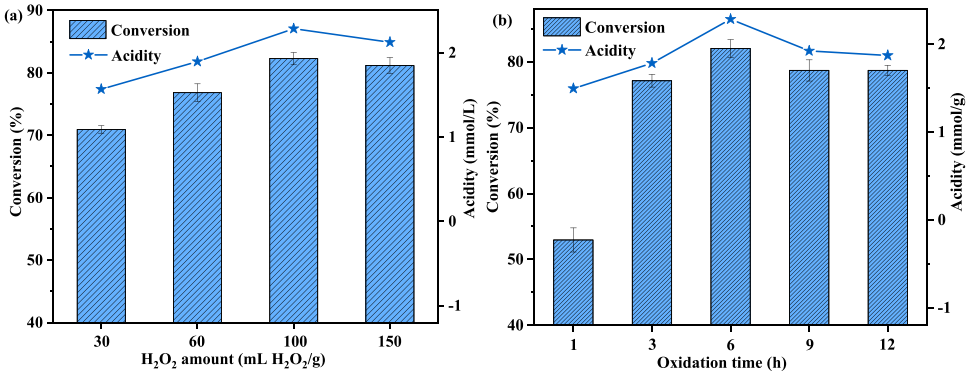

Fig. 3. Influence of H_2O_2 amount (a) and oxidation time (b) on catalytic activity (δ=10 wt%, ζ= 15, φ= 70 °C, τ= 4 h).

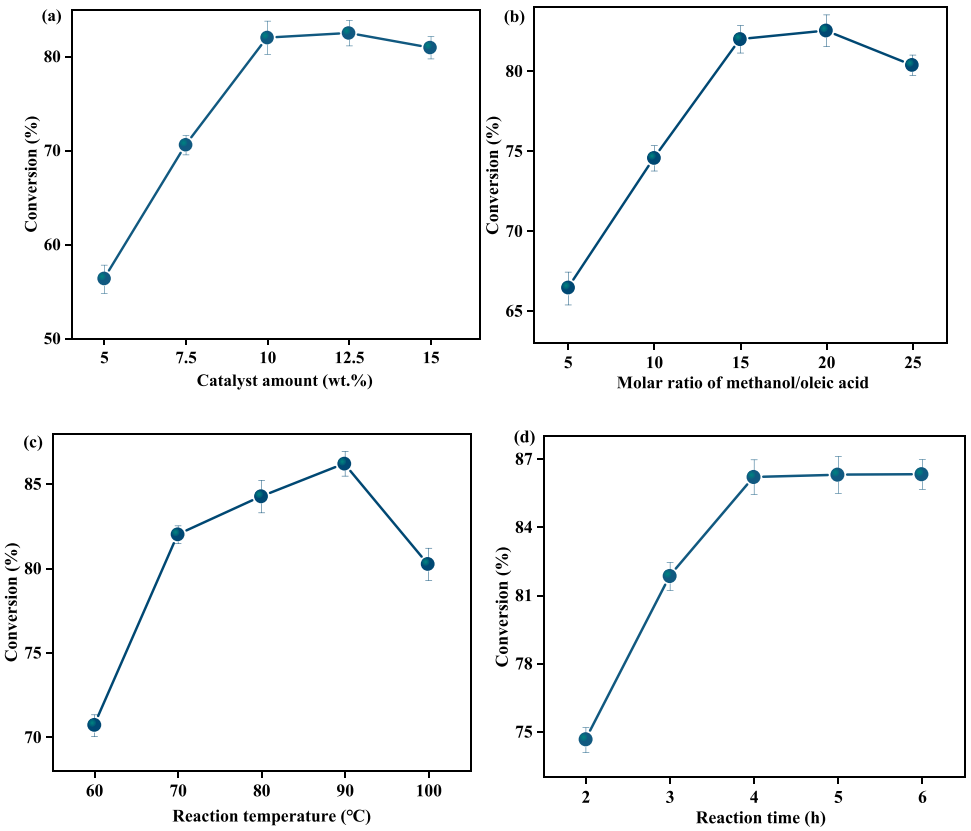

Fig. 4. Effects of various esterification parameters on catalytic activity. (a) Catalyst amount (ζ= 10, φ= 70 °C, τ= 4 h); (b) Molar ratio of methanol/oleic acid (δ= 10 wt%, φ= 70 °C, τ= 4 h); (c) Reaction temperature (δ= 10 wt%, ζ= 8, τ =4 h); (d) Reaction time (δ= 10 wt%, ζ= 8, φ= 90 °C).

of 100 mL H_2O_2/g is selected for next step.

It can be seen from Fig. 3**(b)** the oxidation time imposes profound influence on catalytic activity. In detail, the catalytic activity is only 52.94 %, when the oxidation time is 1 h. Then prolonging oxidation time from 3 h to 6 h, the catalytic activity is accordingly aggrandized from 77.11 % to 82.28 %. However, the catalytic activity is declined as the oxidation time is further extended to 9 h and 12 h. This demonstrates increasing oxidation time during a rational range can promote the formation of Brønsted acid sites. While excessive oxidation time would impair the parent structure of UiO–66–$(SH)_2$ thus leading to decrement of active centers. The acidity variation tendency is identical to that of conversion, where the maximum acidity is achieved at 6 h. Thereby, the oxidation time of 6 h is selected to obtain active sites.

Consequently, the optimum catalyst preparation condition is H_2O_2 amount of 100 mL H_2O_2/g mL and oxidization tine of 6 h.

3.2. Effects of esterification parameters on conversion

It can be seen from Fig. 4**(a)** the esterification conversion is monotonically increased from 46.12 % to 82.5 % as catalyst amount ranging from 5 wt% to 12.5 wt%. The active site is in parallel relationship with catalyst amount, namely, more active site is obtained with higher catalyst amount (Li et al., 2021b). However, as the catalyst amount is over 12.5 wt%, the conversion is tardily decreased to 80.95 % with catalyst amount of 15 wt%. This is probably caused by viscosity increment of reaction medium, thus increasing mass transfer resistance between reactants and catalyst (Barros et al., 2020). Meanwhile, it is ought to be noted that the conversion increment is merely 0.49 % when the catalyst amount is increased from 10 wt% to 12.5 wt%. From the view of economy, catalyst amount of 10 wt% is selected for further study.

Owing to esterification is a reversible reaction, the equilibrium point could be shifted to the right direction of biodiesel production by enlarging methanol amount (Masteri-Farahani et al., 2020). Specifically, the conversion is increased from 66.42 % to 82.55 % with increasing molar ratio of methanol/oleic acid from 5 to 20 (Fig. 4**(b)**). Yet the conversion is reduced to 80.36 % as the molar ratio of methanol/oleic acid is 25. This is due to excessive methanol would dilute the catalyst concentration, thus reducing the effective contact between reactants and active site (Sangar et al., 2019). Notably, the conversion is only 0.45 % as molar ratio of methanol/oleic acid of 20 in comparison to that of 15, and the excessive methanol would raise the recovery cost. Thereby, the molar ratio of methanol/oleic acid is set as 15 for further study.

High temperature is in favor of esterification owing to it is an endothermic reaction (Li et al., 2021a). As depicted in Fig. 4**(c)**, the conversion is only 70.69 % at 60 °C and the maximum conversion of 86.21 % is obtained at 90 °C. However, the conversion is decreased to 80.25 % at 100 °C. In theory, high temperature is in favor of accelerating mass transfer of reactants on catalyst surface. While excessive temperature would expedite methanol evaporation. As a result, the bubbles are generated and wrapped around catalyst, hindering the contact between

Table 1
Catalytic activity comparison of different solid acids.

Catalysts	Feedstock and reactions	Conversion (%)
UiO–66–$(SH)_2$	Molar ratio of methanol/oleic acid of 10, catalyst amount of 8 wt% at 70 °C for 4 h	65.25
UiO–66–$(SO_3H)_2$	Molar ratio of methanol/oleic acid of 15, catalyst amount of 10 wt% at 90 °C for 4 h	86.21
ZrO_2	Molar ratio of methanol/oleic acid of 12, catalyst amount of 7 wt% at 70 °C for 9 h	82 (Marchetti et al., 2007)
SO_4^{2-}/ZrO_2	Molar ratio of methanol/ palmitic acid of 40, catalyst amount of 10 wt% at 95 °C for 6 h	91 (Chen et al., 2013)
SO_4^{2-}/ZrO_2	Molar ratio of methanol/ oleic acid of 40:1, catalyst amount of 0.5 g at 60 °C for 12 h	90 (Patel et al., 2013)

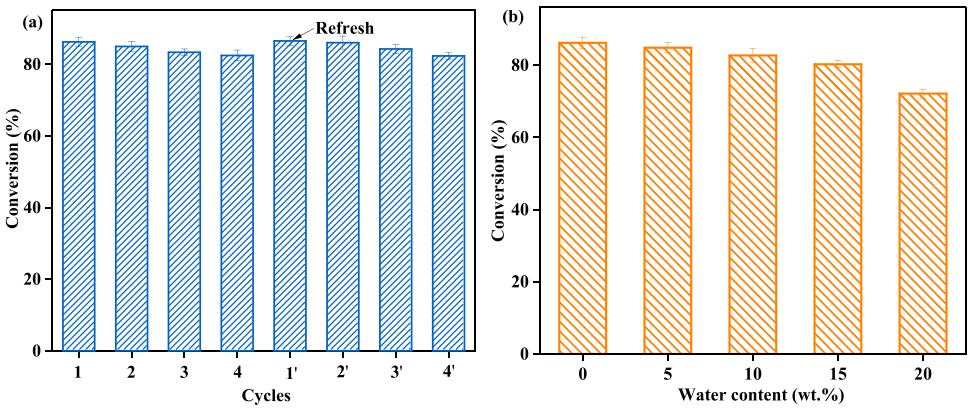

Fig. 5. Reusability (a) and water resistance (b) of UiO–66–$(SO_3H)_2$. (δ=10 wt%, ζ= 15, φ= 90 °C, τ= 4 h).

catalyst and reactants and leading to conversion decrement (Alismaeel et al., 2018). In addition, higher temperature causes much energy consumption, hence, the reaction temperature is selected as 90 °C.

Once the above three parameters are confirmed, the corresponding equilibrium time is determined. It can be observed from Fig. 4**(d)** the conversion is increased with prolonging reaction time from 2 h to 4 h. After that, the conversion increment is negligible indicating the equilibrium point is obtained at 4 h.

In summary, the optimal esterification parameters are catalyst amount of 10 wt%, molar ratio of methanol/oleic acid of 15, reaction temperature of 90 °C, and reaction time of 4 h. In comparison to the reported solid acid (Table 1), UiO–66–$(SO_3H)_2$ possesses favorable catalytic activity. For instance, UiO–66–$(SO_3H)_2$ achieves the comparable conversion in comparison to that of SO_4^{2-}/ZrO_2, yet, UiO–66–$(SO_3H)_2$ could evidently reduce the methanol and reaction time. This confirms UiO–66–$(SO_3H)_2$ is an efficient catalyst for biodiesel production.

In order to further verify the promising catalytic activity of UiO–66–$(SO_3H)_2$, the kinetic parameters of activation energy and reaction order are calculated, which is specified in the supplementary material. The average reaction order for oleic acid is 0.011, this indicates the reaction rate is almost irrelevant with the oleic acid concentration. The activation energy is calculated as 15.35 kJ/mol. According to the reported literature, the activation energy for esterification of oleic acid and methanol catalyzed by 4-dodecylbenzenesulfonic acid was 58.5 kJ/mol (Alegría and Cuellar, 2015). El Saey et al. (El Saey et al., 2023) used the sulfonated biochar to catalyze oleic acid and methanol with 7.5 wt% catalyst amount and molar ratio of methanol to oleic acid of 12 in 2 h, the corresponding activation energy was 29.93 kJ/mol. In comparison, UiO–66–$(SO_3H)_2$ evidently reduces the activation energy of esterification of oleic acid and methanol. Therefore, UiO–66–$(SO_3H)_2$ is a highly efficient solid acid catalyst for esterification on the purpose of biodiesel production.

3.3. Catalyst reusability and water resistance

To further evaluate the reusability of UiO–66–$(SO_3H)_2$, the catalyst is isolated via centrifugation and used directly for fresh oleic acid and methanol without further treatment. As shown in Fig. 5**(a)**, UiO–66–$(SO_3H)_2$ exhibits favorable reusability performance, where only 3.54 % conversion decrement is observed during four cycles. It is reported that the catalytic activity decrement was principally originated from the active sites leaching (Alcañiz-Monge et al., 2018). To refresh the catalytic activity, the used catalyst is purified by cyclohexane and ethanol to eliminate the absorbed methyl ester and other organic impurities, which is then acidified by 0.1 mol/L dilute sulfuric acid for 30 min to regenerate acid site. As expected, the catalytic activity is assuredly recovered, where the conversion of 86.48 % is achieved with molar ratio of methanol/oleic acid of 10:1, catalyst amount of 8 wt% at 70 °C for 4 h.

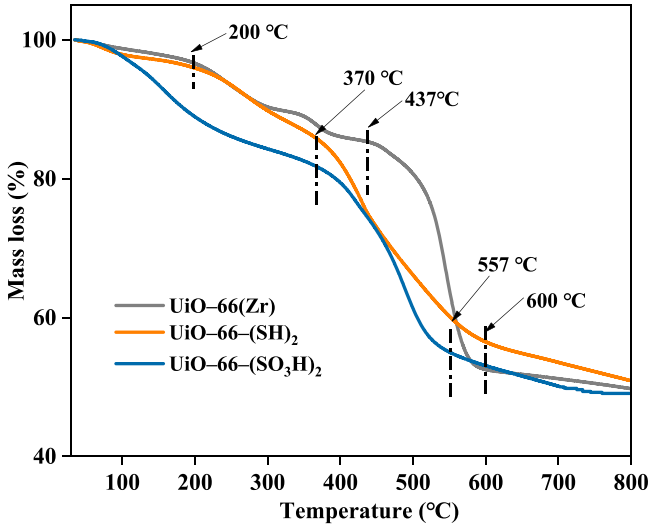

Fig. 6. TG curves of UiO–66(Zr), UiO–66–$(SH)_2$, and UiO–66–$(SO_3H)_2$.

This demonstrates the catalytic activity of UiO–66–$(SO_3H)_2$ could be simply regenerated.

In addition, hot filtration test is conducted to verify the stability of UiO–66–$(SO_3H)_2$, in which the UiO–66–$(SH)_2$ is also examined for comparison. In detail, 4 g UiO-66-$(SH)_2$ and UiO-66-$(SO_3H)_2$ are mixed with certain amount of methanol under each optimal conditions as presented in Table 1. After that, UiO–66–$(SH)_2$ and UiO–66–$(SO_3H)_2$ are separated from methanol, the filtered methanol is used react with oleic acid. Result indicates the conversion obtained by the filtered methanol from UiO-66-$(SH)_2$ and UiO-66-$(SO_3H)_2$ are 1.65 % and 2.97 %, respectively. On the other hand, the isolated UiO-66-$(SH)_2$ and UiO–66–$(SO_3H)_2$ are used to catalyze fresh methanol and oleic acid under corresponding optimal conditions, the obtained conversion is 64.76 % and 86.03 %, respectively, which is basically same to their original catalytic activity. It can be reasonably concluded that UiO–66–$(SO_3H)_2$ is the heterogeneous catalyst with satisfying stability.

On account of water is the by-product of esterification (**Eq. 1**), it leads to the active sites immersing in water. Thereby, water resistance is also a critical property for solid acid and it is necessary to investigate the influence of water on catalytic activity of UiO–66–$(SO_3H)_2$. As can be observed from Fig. 5**(b)**, the conversion of 84.88 % and 82.73 % is achieved with water content of 5 wt% and 10 wt%, respectively. It manifests UiO–66–$(SO_3H)_2$ is barely affected by water when water content is less than 10 wt%. While, the conversion is decreased by 6.62 % with 20 wt% water content, this is ascribed to the partial hydrolysis of $–SO_3H$. Park et al. (2010) previously reported the catalytic activity of

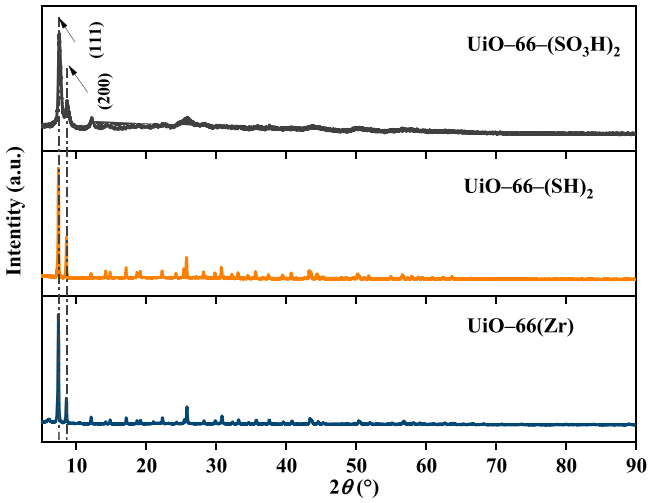

Fig. 7. XRD patterns of UiO–66(Zr), UiO–66–$(SH)_2$, and UiO–66–$(SO_3H)_2$.

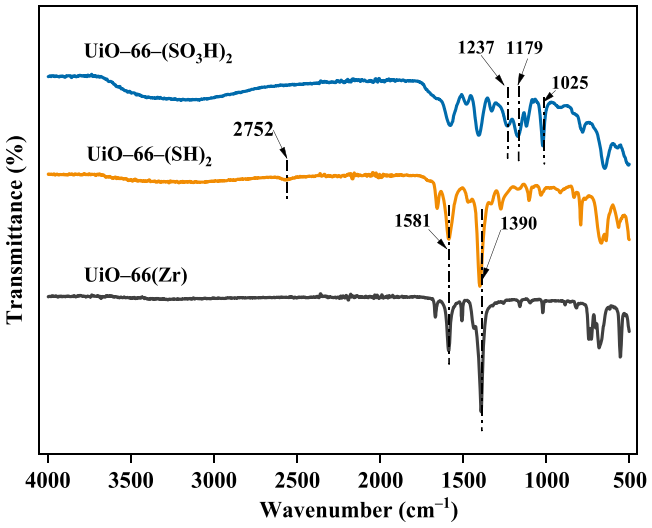

Fig. 8. FTIR spectra of UiO–66(Zr), UiO–66–$(SH)_2$ and UiO–66–$(SO_3H)_2$.

sulphuric acid was rapidly reduced by 76 % with 20 wt% water content. By contrast, UiO–66–$(SO_3H)_2$ owns favorable water resistance for biodiesel production.

In light of the excellent stability, it is essential to characterize UiO–66–$(SO_3H)_2$ to reveal the relationship between physicochemical structure and catalytic activity.

3.4. Catalyst characterizations

As depicted in Fig. 6, the thermal stability shifts to low temperature region once UiO–66(Zr) is modified into UiO–66–$(SH)_2$ and UiO–66–$(SO_3H)_2$. In detail, both UiO–66(Zr) and UiO–66–$(SH)_2$ exhibits three mass loss steps, the first mass loss about 3.2 % is originated from elimination of residual water and DMF. The second mass loss of UiO–66–$(SH)_2$ occurs at 200 °C is attributed the dehydroxylation of $Zr_6O_4(OH)_4$ clusters resulting in Zr_6O_6 formation (Lozano et al., 2018), which is ended at 370 °C. While for UiO–66(Zr), the second mass loss is terminated at 437 °C. The third mass loss step initiated from 370 °C to 592 °C is ascribed to the framework collapse and organic ligand degradation. Since –SH is oxidized into $–SO_3H$, the thermal stability of UiO–66–$(SO_3H)_2$ is further weakened, the first mass loss of 12.3 % is originated from the elimination of physically adsorbed water owing to the strong hydrophilicity of $–SO_3H$. The second mass loss occurred between 370 °C–557 °C is aroused by structure collapse. Even so, the thermal stability of UiO–66–$(SO_3H)_2$ is still satisfying for esterification which is normally conducted below 120 °C.

It can be observed from Fig. 7, UiO–66–$(SH)_2$, UiO–66–$(SO_3H)_2$ and UiO–66(Zr) exhibit similar XRD pattern, and the diffraction peaks are appeared at same diffraction angle. In detail, 2θ at 7.34° and 8.48° are the characteristic peaks of UiO–66(Zr) (CCDC 733458) (Li et al., 2019; Sarango-Ramírez et al., 2020). The identical diffraction peaks at 7.34° and 8.48° are also detected in UiO–66–$(SH)_2$, which are attributed to the crystal planes (111) and (200), confirming UiO–66–$(SH)_2$ is topologically equivalent with the face–centered cubic lattice of UiO–66(Zr). Furthermore, UiO–66–$(SO_3H)_2$ also exhibits (111) and (200) crystal planes, indicating the crystal structure is basically stable. However, it can be seen the prepared UiO–66(Zr) possesses higher crystallinity than that of UiO–66–$(SO_3H)_2$, which is attributed to organic ligand of UiO–66–$(SO_3H)_2$ is hung with $–SO_3H$ thus leading to the decrease of crystallinity. In addition, UiO–66–$(SO_3H)_2$ has no obvious characteristic peak of sulfonic acid groups, it might attributed to the high dispersion of sulfonic acid groups in the framework structure, further ensuring the high utilization of active sites.

To further confirm the presence of –SH and $–SO_3H$ in UiO–66–$(SH)_2$ and UiO–66–$(SO_3H)_2$, FTIR spectra are depicted in Fig. 8. It can be clearly seen that the spectra of UiO–66–$(SH)_2$ and UiO–66–$(SO_3H)_2$ are similar to that of UiO–66(Zr), where the stretching vibration of Zr–O–Zr, the symmetric vibrations of carboxyl (O═C–O) are recorded at 1390 cm^{-1} and 1581 cm^{-1} (Li et al., 2021a), respectively. In addition, the stretching vibration at 2752 cm^{-1} is detected in UiO–66–$(SH)_2$ corresponding to –SH, which is invisible in the spectrum of UiO–66(Zr). By contrast, the vibration band of –SH is disappeared in UiO–66–$(SO_3H)_2$. Meanwhile, the asymmetric and symmetric stretching vibration band of S═O is shown at 1237 cm^{-1} and 1179 cm^{-1} in UiO–66–$(SO_3H)_2$ (Chen et al., 2019), respectively. The band at 1025 cm^{-1} is assigned to S–O stretching vibration for UiO–66–$(SO_3H)_2$ (Fernández-Morales et al., 2019), verifying –SH is oxidized and acidified to $–SO_3H$. Therefore, it is verified that sulfonic acid and organic ligand are connected by covalent

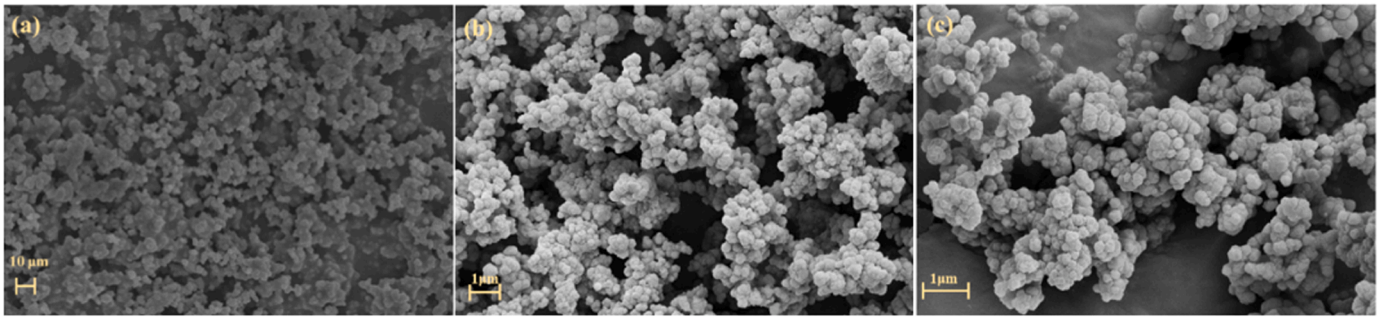

Fig. 9. Surface morphologies of (a) UiO–66(Zr), (b) UiO–66–$(SH)_2$ and (c) UiO–66–$(SO_3H)_2$.

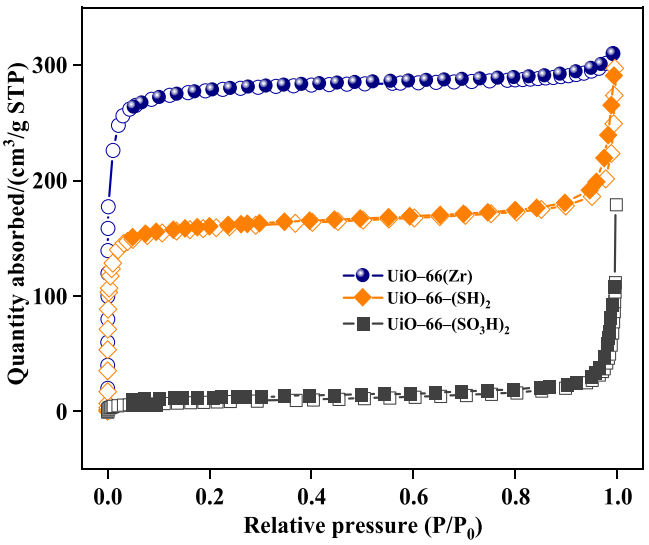

Fig. 10. N_2 absorption/desorption isotherm curves of UiO–66(Zr), UiO–66–$(SH)_2$, and UiO–66–$(SO_3H)_2$.

Table 2
Surface area, pore volume, and average pore diameter of catalysts.

Sample	Specific surface area (m^2/g)	Pore volume (cm^3/g)	Average pore diameter (nm)
UiO–66(Zr)	861.82	0.46	2.17
UiO–66–$(SH)_2$	454.46	0.36	2.34
UiO–66–$(SO_3H)_2$	32.18	0.15	10.53
$SO_4^{2-}/ZrO_2/Al_2O_3$ (Rahmani Vahid et al., 2018)	13.2	0.029	9.7
SO_4^{2-}/C (Mardhiah et al., 2017)	1.92	0.0032	6.67
1.5–SZ–MT (Yang et al., 2020)	8.9	0.03	21.01

bond, in which the eight–electron stable structure is formed between C and S (Zheng et al., 2021).

The surface morphology is also compared between UiO–66–$(SH)_2$ and UiO–66–$(SO_3H)_2$ as illustrated in Fig. 9. Even though the replacement of terephthalic acid, the octahedral structure is still observed in UiO–66–$(SH)_2$ (Fig. 9 **(b)**) and UiO–66–$(SO_3H)_2$ (Fig. 9 **(c)**), which is similar to that of UiO–66(Zr) (Fig. 9 **(a)**), confirming the structure of UiO–66–$(SH)_2$ and UiO–66–$(SO_3H)_2$ is inherited from UiO–66(Zr), this is in accordance with XRD result. It also verifies the crystal structure remains stable during the oxidation process. Nevertheless, it seems the particles of UiO–66–$(SH)_2$ and UiO–66–$(SO_3H)_2$ are stuck together, which is might attributed to the hydrogen bond generated among –SO_3H.

As depicted in Fig. 10, the isotherm pattern of UiO–66–$(SH)_2$ is similar to that of UiO–66(Zr), which is the type I isotherm pattern equipped with hysteresis loop, indicating it is a micro-pore material. The absorbing quantity of UiO–66–$(SH)_2$ is evidently lower than that of UiO–66(Zr). As a result, the surface area and pore volume of UiO–66–$(SH)_2$ are 454.46 m^2/g and 0.36 cm^3/g (Table 2), respectively.

After being oxidized and acidified, the obtained UiO–66–$(SO_3H)_2$ shows type III isotherm pattern, its specific surface area and pore volume are decreased to 32.18 m^2/g and 0.15 cm^3/g. Nonetheless, the pore diameter of UiO–66–$(SO_3H)_2$ is expanded to 10.52 nm, this is beneficial to mass transfer thus accelerating esterification. In comparison to UiO–66(Zr), the surface area and pore volume of both UiO–66–$(SH)_2$ and UiO–66–$(SO_3H)_2$ are vastly decreased due to the porosity is occupied by the connected sulfydryl (–SH) and –SO_3H. Even so, UiO–66–

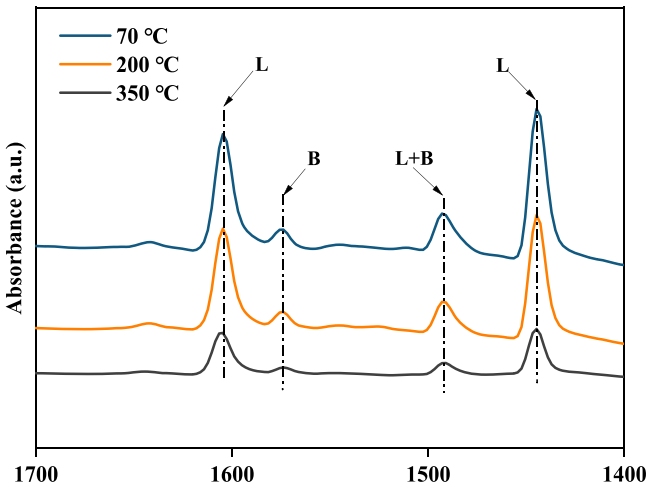

Fig. 11. Py–FTIR spectra of UiO–66–$(SO_3H)_2$.

Table 3
Lewis acid and Brønsted acid amounts of UiO–66, UiO–66–$(SH)_2$, and UiO–66–$(SO_3H)_2$.

Sample	Desorbed temperature (°C)	Acid amount (μmol/g)		
		B acid	L acid	Total acid
UiO–66	70	2.83	27.55	30.38
	200	1.62	15.12	17.04
	350	0.32	2.97	3.29
UiO–66–$(SH)_2$	70	3.06	32.65	35.71
	200	1.86	20.57	22.43
	350	0.59	10.99	11.58
UiO–66–$(SO_3H)_2$	70	3.74	69.06	72.81
	200	2.17	56.37	58.54
	350	0.97	21.93	22.90

$(SO_3H)_2$ still provides considerable specific surface area and pore volume in comparison to the congeneric solid acid (Table 2). For instance, the surface area and pore volume of $SO_4^{2-}/ZrO_2/Al_2O_3$ was merely 13.2 m^2/g and 0.029 cm^3/g. By contrast, UiO–66–$(SO_3H)_2$ could achieve full contact between active site and reactants, thus enhancing catalytic activity (Björk et al., 2017).

UiO–66–$(SO_3H)_2$ is further characterized via py–FTIR to evaluate the acid site property in depth. It can be observed from Fig. 11, UiO–66–$(SO_3H)_2$ is equipped with Lewis (L) acid and Brønsted (B) acid. Thereinto, L acid is found at 1600 cm^{-1} and 1450 cm^{-1} originating from the unsaturated coordination of Zr. Additionally, the absorption band at 1540 cm^{-1} is assigned to B acid due to the existence of –SO_3H (Li et al., 2021b). As for the absorption peak at 1490 cm^{-1}, it is a combination of L acid and B acid (Zhang et al., 2019). The existence of B acid is beneficial to protonating carboxylic acid to generate more positive charge of carbonyl carbon, which enhances the nucleophilic reaction with alcohol and increases esterification conversion. While the L acid could prevent active site from hydration (Shu et al., 2019), this is the reason for the promising reusability of UiO–66–$(SO_3H)_2$ shown in Fig. 5. As expected, the amount of L acid is evidently higher than that of B acid on account of the larger corresponding peak area. Based on the reported literature (Zhang et al., 2009), the strength order of acid site is determined by pyridine evacuation temperature: weak (50–150 °C) < medium (150–300 °C) < strong (350 °C).

As presented in Table 3, the acidity amount of UiO–66–$(SH)_2$ is obviously higher than that of UiO-66 when the organic ligand is changed from terephthalic acid to 2,5–dimercaptoterephthalic acid. Once the sulfydryl is further oxidatively protonated, both L acid and B acid of UiO–66–$(SO_3H)_2$ are obviously higher than that of UiO–66–$(SH)_2$ at different acid strength. For instance, the L acid of UiO–66–$(SO_3H)_2$ is

Table 4
Biodiesel property comparison with EN 14214 standard.

Index	Biodiesel in this study	EN 14214 standard
Cetane number	59	>51
Kinetic viscosity (40 °C, mm^2/s)	4.1	3.5–5.0
Density (15 °C, g/cm^3)	0.89	0.86–0.9
Flash point (°C)	122	120
Residual carbon (%)	0.005	<0.03

about 2 times higher than that of UiO–66–$(SH)_2$, this is beneficial to improving catalyst stability.

3.5. Biodiesel property

Physicochemical properties of cetane number, viscosity, density, flash point, residual carbon for the biodiesel obtained by the catalyst of UiO–66–$(SO_3H)_2$ is evaluated and compared with that of EN 14214 standard (Table 4). Satisfyingly, the biodiesel meets all of EN 14214 standard limits, especially the cetane number, it is obviously higher than that of EN 14214 standard, which means it possesses good firing performance and homogeneous combustion in diesel engine. Therefore, the biodiesel obtained in this study could be directly used as transport fuel.

4. Conclusions

In this study, the organic ligand of UiO–66(Zr) is replaced with 2,5–dimercaptoterephthalic acid, and then the –SH is oxidized and acidified into –SO_3H. With this strategy, –SO_3H is connected to organic ligand through covalent bond with formation of UiO–66–$(SO_3H)_2$. It inherits the original structure from UiO-66(Zr) and the acidity is 2.28 mmol/g, which is beneficial to enhancing catalytic activity. As a result, the maximum esterification conversion of 86.21 % is achieved by UiO–66–$(SO_3H)_2$ with catalyst amount of 10 wt%, molar ratio of methanol/oleic acid of 15 at 90 °C for 4 h. The conversion decrement is merely reduced by 3.54 % during four successive cycles, the physicochemical property of the obtained biodiesel satisfies the EN 14214 standard. This study provides a new approach to synthesize stable and efficient solid acid catalyst for biodiesel production.

CRediT authorship contribution statement

Shijie Li: Formal analysis. **Xiaoling Ma:** Resources, Supervision. **Hewei Yu:** Resources. **Guoning Li:** Formal analysis. **Tianyu Wang:** Investigation. **Hui Li:** Methodology, Writing – original draft. **Huijun Chu:** Investigation. **Yaning Zhang:** Data curation, Formal analysis. **Samuel Lalthazuala Rokhum:** Data curation, Writing – review & editing. **Min Guo:** Resources. **Qiangqiang Xiao:** Validation.

Declaration of Competing Interest

The authors declare that they have no known competing financial interests or personal relationships that could have appeared to influence the work reported in this paper.

Acknowledgements

This work is supported by National Natural Science Foundation of China (52376198, 51806126), Excellent Youth Science Fund in Shandong Province (ZR2023YQ046), Young Talent of Lifting Engineering for Science and Technology in Shandong (SDAST2021qt09), Development Plan of Youth Innovation Team of Shandong Provincial Colleges and Universities (2022KJ209), Talent Research Project of Qilu University of Technology (Shandong Academy of Sciences) (2023RCKY170), and Postdoctoral Innovation Project of Shandong Province (202102034).

Appendix A. Supporting information

Supplementary data associated with this article can be found in the online version at doi:10.1016/j.cherd.2024.04.040.

References

Alcañiz-Monge, J., Bakkali, B.E., Trautwein, G., Reinoso, S., 2018. Zirconia-supported tungstophosphoric heteropolyacid as heterogeneous acid catalyst for biodiesel production. Appl. Catal. B: Environ. 224, 194–203.
Alegría, A., Cuellar, J., 2015. Esterification of oleic acid for biodiesel production catalyzed by 4-dodecylbenzenesulfonic acid. Appl. Catal. B: Environ. 179, 530–541.
Alismaeel, Z.T., Abbas, A.S., Albayati, T.M., Doyle, A.M., 2018. Biodiesel from batch and continuous oleic acid esterification using zeolite catalysts. Fuel 234, 170–176.
Alvear-Daza, J.J., Pasquale, G.A., Rengifo-Herrera, J.A., Romanelli, G.P., Pizzio, L.R., 2021. Mesoporous activated carbon from sunflower shells modified with sulfonic acid groups as solid acid catalyst for itaconic acid esterification. Catal. Today 372, 51–58.
Andreoli, S.P., 1993. Captopril scavenges hydrogen peroxide and reduces, but does not eliminate, oxidant-induced cell injury. Am. J. Physiol. -Ren. Physiol. 264, F120–F127.
Barros, de S., Pessoa Junior, S., Sá, W.A.G., Takeno, I.S.C., Nobre, M.L., Pinheiro, F.X., Manzato, W., Iglauer, L., de Freitas, S., F.A, 2020. Pineapple (Ananás comosus) leaves ash as a solid base catalyst for biodiesel synthesis. Bioresour. Technol. 312, 123569.
Björk, E.M., Militello, M.P., Tamborini, L.H., Coneo Rodriguez, R., Planes, G.A., Acevedo, D.F., Moreno, M.S., Odén, M., Barbero, C.A., 2017. Mesoporous silica and carbon based catalysts for esterification and biodiesel fabrication-The effect of matrix surface composition and porosity. Appl. Catal. A: Gen. 533, 49–58.
Chen, G., Guo, C.-Y., Qiao, H., Ye, M., Qiu, X., Yue, C., 2013. Well-dispersed sulfated zirconia nanoparticles as high-efficiency catalysts for the synthesis of bis(indolyl) methanes and biodiesel. Catal. Commun. 41, 70–74.
Chen, T.-F., Han, S.-Y., Wang, Z.-P., Gao, H., Wang, L.-Y., Deng, Y.-H., Wan, C.-Q., Tian, Y., Wang, Q., Wang, G., Li, G.-S., 2019. Modified UiO-66 frameworks with methylthio, thiol and sulfonic acid function groups: The structure and visible-light-driven photocatalytic property study. Appl. Catal. B: Environ. 259, 118047.
Cong, W.-j, Yang, J., Zhang, J., Fang, Z., Miao, Z.-d, 2023. A green process for biodiesel and hydrogen coproduction from waste oils with a magnetic metal-organic framework derived material. Biomass-.-. Bioenergy 175, 106871.
da Silva, M.J., Rodrigues, A.A., 2020. Metal silicotungstate salts as catalysts in furfural oxidation reactions with hydrogen peroxide. Mol. Catal. 493, 111104.
El Saey, H.S., Abo El Naga, A.O., El Saied, M., Shaban, S.A., Abdel-Gawad, S.A., Salih, S. A., 2023. Kinetic and thermodynamic studies on the esterification of oleic acid with methanol over sulfonated biochar catalyst derived from waste tea dregs. Biomass-.-. Bioenergy 176, 106892.
Fernández-Morales, J.M., Lozano, L.A., Castillejos-López, E., Rodríguez-Ramos, I., Guerrero-Ruiz, A., Zamaro, J.M., 2019. Direct sulfation of a Zr-based metal-organic framework to attain strong acid catalysts. Microporous Mesoporous Mater. 290, 109686.
Gaikwad, S., Kim, Y., Gaikwad, R., Han, S., 2022. Enhanced VOC adsorption capacity on MOF thin layer with reduced particle size by cryogrinding and microwave method. J. Environ. Chem. Eng. 10, 107567.
Gouda, S.P., Ngaosuwan, K., Assabumrungrat, S., Selvaraj, M., Halder, G., Rokhum, S.L., 2022. Microwave assisted biodiesel production using sulfonic acid-functionalized metal-organic frameworks UiO-66 as a heterogeneous catalyst. Renew. Energy 197, 161–169.
Gouda, S.P., Shi, D., Basumatary, S., Li, H., Piloto-Rodríguez, R., Rokhum, S.L., 2024. Sulfamic acid modified UiO-66 metal-organic framework for biodiesel production: Process optimization using response surface methodology, kinetics, and thermodynamic study. Chem. Eng. J. 480, 148154.
Jrad, A., Hmadeh, M., Awada, G., Chakleh, R., Ahmad, M., 2021. Efficient biofuel production by MTV-UiO-66 based catalysts. Chem. Eng. J. 410, 128237.
Li, Z., Chen, H., Chen, C., Guo, Q., Li, X., He, Y., Wang, H., Feng, N., Wan, H., Guan, G., 2019. High dispersion of polyethyleneimine within mesoporous UiO-66s through pore size engineering for selective CO2 capture. Chem. Eng. J. 375, 121962.
Li, H., Chu, H., Ma, X., Wang, G., Liu, F., Guo, M., Lu, W., Zhou, S., Yu, M., 2021a. Efficient heterogeneous acid synthesis and stability enhancement of UiO-66 impregnated with ammonium sulfate for biodiesel production. Chem. Eng. J. 408, 127277.
Li, H., Han, Z., Liu, F., Li, G., Guo, M., Cui, P., Zhou, S., Yu, M., 2021b. Esterification catalyzed by an efficient solid acid synthesized from PTSA and UiO-66(Zr) for biodiesel production. Faraday Discuss. 231, 342–355.
Li, H., Wang, J., Ma, X., Wang, Y., Li, G., Guo, M., Cui, P., Lu, W., Zhou, S., Yu, M., 2021c. Carbonized MIL−100(Fe) used as support for recyclable solid acid synthesis for biodiesel production. Renew. Energy 179, 1191–1203.
Liu, X., Pan, H., Zhang, H., Li, H., Yang, S., 2019. Efficient Catalytic Upgradation of Bio-Based Furfuryl Alcohol to Ethyl Levulinate Using Mesoporous Acidic MIL-101(Cr). ACS Omega 4, 8390–8399.
Lozano, L.A., Iglesias, C.M., Faroldi, B.M.C., Ulla, M.A., Zamaro, J.M., 2018. Efficient solvothermal synthesis of highly porous UiO-66 nanocrystals in dimethylformamide-free media. J. Mater. Sci. 53, 1862–1873.
Lu, P., Li, H., Li, M., Chen, J., Ye, C., Wang, H., Qiu, T., 2022. Ionic liquid grafted NH_2-UiO-66 as heterogeneous solid acid catalyst for biodiesel production. Fuel 324, 124537.

Marchetti, J.M., Miguel, V.U., Errazu, A.F., 2007. Heterogeneous esterification of oil with high amount of free fatty acids. Fuel 86, 906–910.
Mardhiah, H.H., Ong, H.C., Masjuki, H.H., Lim, S., Pang, Y.L., 2017. Investigation of carbon-based solid acid catalyst from Jatropha curcas biomass in biodiesel production. Energy Convers. Manag. 144, 10–17.
Masteri-Farahani, M., Hosseini, M.-S., Forouzeshfar, N., 2020. Propyl-SO_3H functionalized graphene oxide as multipurpose solid acid catalyst for biodiesel synthesis and acid-catalyzed esterification and acetalization reactions. Renew. Energy 151, 1092–1101.
Ning, Y., Niu, S., Han, K., Lu, C., 2020. Catalytic capability of phosphotungstic acid supported on bamboo activated carbon in esterification for biodiesel production with density functional theory. Biomass-.-. Bioenergy 143, 105873.
Park, J.-Y., Wang, Z.-M., Kim, D.-K., Lee, J.-S., 2010. Effects of water on the esterification of free fatty acids by acid catalysts. Renew. Energy 35, 614–618.
Patel, A., Brahmkhatri, V., Singh, N., 2013. Biodiesel production by esterification of free fatty acid over sulfated zirconia. Renew. Energy 51, 227–233.
Prinsen, P., Luque, R., González-Arellano, C., 2018. Zeolite catalyzed palmitic acid esterification. Microporous Mesoporous Mater. 262, 133–139.
Qi, G., Wang, Q., Xu, J., Trébosc, J., Lafon, O., Wang, C., Amoureux, J.-P., Deng, F., 2016. Synergic Effect of Active Sites in Zinc-Modified ZSM-5 Zeolites as Revealed by High-Field Solid-State NMR Spectroscopy. Angew. Chem. Int. Ed. 55, 15826–15830.
Qiu, J.-L., Su, J., Muhammad, N., Zheng, W.-T., Yue, C.-L., Liu, F.-Q., Zuo, J.-L., Ding, Z.-J., 2022. Facile encapsulating Ag nanoparticles into a Tetrathiafulvalene-based Zr-MOF for enhanced Photocatalysis. Chem. Eng. J. 427, 131970.
Rahmani Vahid, B., Saghatoleslami, N., Nayebzadeh, H., Toghiani, J., 2018. Effect of alumina loading on the properties and activity of SO_4^{2-}/ZrO_2 for biodiesel production: Process optimization via response surface methodology. J. Taiwan Inst. Chem. Eng. 83, 115–123.
Ruatpuia, J.V.L., Halder, G., Mohan, S., Gurunathan, B., Li, H., Chai, F., Basumatary, S., Lalthazuala Rokhum, S., 2023. Microwave-assisted biodiesel production using ZIF-8 MOF-derived nanocatalyst: A process optimization, kinetics, thermodynamics and life cycle cost analysis. Energy Convers. Manag. 292, 117418.
Sangar, S.K., Syazwani, O.N., Farabi, M.S.A., Razali, S.M., Shobhana, G., Teo, S.H., Taufiq-Yap, Y.H., 2019. Effective biodiesel synthesis from palm fatty acid distillate (PFAD) using carbon-based solid acid catalyst derived glycerol. Renew. Energy 142, 658–667.
Sarango-Ramírez, M.K., Lim, D.-W., Kolokolov, D.I., Khudozhitkov, A.E., Stepanov, A.G., Kitagawa, H., 2020. Superprotonic Conductivity in Metal-Organic Framework via Solvent-Free Coordinative Urea Insertion. J. Am. Chem. Soc. 142, 6861–6865.
Shu, Q., Zou, W., He, J., Lesmana, H., Zhang, C., Zou, L., Wang, Y., 2019. Preparation of the F^--SO_4^{2-}/MWCNTs catalyst and kinetic studies of the biodiesel production via esterification reaction of oleic acid and methanol. Renew. Energy 135, 836–845.
Udenigwe, C.C., Udechukwu, M.C., Yiridoe, C., Gibson, A., Gong, M., 2016. Antioxidant mechanism of potato protein hydrolysates against in vitro oxidation of reduced glutathione. J. Funct. Foods 20, 195–203.
Valenzano, L., Civalleri, B., Chavan, S., Bordiga, S., Nilsen, M.H., Jakobsen, S., Lillerud, K.P., Lamberti, C., 2011. Disclosing the Complex Structure of UiO-66 Metal Organic Framework: A Synergic Combination of Experiment and Theory. Chem. Mater. 23, 1700–1718.
Wang, T., Ma, X., Bingwa, N., Yu, H., Wang, Y., Li, G., Guo, M., Xiao, Q., Li, S., Zhao, X., Li, H., 2024. A novel bimetallic CaFe-MOF derivative for transesterification: Catalytic performance, characterization, and stability. Energy 292, 130544.
Wang, S., Pu, J., Wu, J., Liu, H., Xu, H., Li, X., Wang, H., 2020. SO_4^{2-}/ZrO_2 as a Solid Acid for the Esterification of Palmitic Acid with Methanol: Effects of the Calcination Time and Recycle Method. ACS Omega 5, 30139–30147.
Wu, Y., Zhang, Y., Chen, R., Zhu, Y., Yan, J., Chen, Y., 2022. Hydroxyl-functionalized & aluminium-modified UiO-66 for highly performance fluorescence detection ClO- in water. J. Solid State Chem. 305, 122690.
Xia, Z., Shi, B., Zhu, W., Lü, C., 2021. Temperature-responsive polymer-tethered Zr-porphyrin MOFs encapsulated carbon dot nanohybrids with boosted visible-light photodegradation for organic contaminants in water. Chem. Eng. J. 426, 131794.
Xie, W., Wan, F., 2019. Immobilization of polyoxometalate-based sulfonated ionic liquids on UiO-66-2COOH metal-organic frameworks for biodiesel production via one-pot transesterification-esterification of acidic vegetable oils. Chem. Eng. J. 365, 40–50.
Yang, H., Zhou, Y., Tong, D., Yang, M., Fang, K., Zhou, C., Yu, W., 2020. Catalytic conversion of cellulose to reducing sugars over clay-based solid acid catalyst supported nanosized SO_4^{2-}-ZrO_2. Appl. Clay Sci. 185, 105376.
Yıldız, T., Erucar, I., 2022. Revealing the performance of bio-MOFs for adsorption-based uremic toxin separation using molecular simulations. Chem. Eng. J. 431, 134263.
Zeppini, P., van den Bergh, J.C.J.M., 2020. Global competition dynamics of fossil fuels and renewable energy under climate policies and peak oil: A behavioural model. Energy Policy 136, 110907.
Zhang, Q., Lei, Y., Li, L., Lei, J., Hu, M., Deng, T., Zhang, Y., Ma, P., 2023. Construction of the novel PMA@Bi-MOF catalyst for effective fatty acid esterification. Sustain. Chem. Pharm. 33, 101038.
Zhang, P., Wu, H., Fan, M., Sun, W., Jiang, P., Dong, Y., 2019. Direct and postsynthesis of tin-incorporated SBA-15 functionalized with sulfonic acid for efficient biodiesel production. Fuel 235, 426–432.
Zhang, X., Zhong, J., Wang, J., Zhang, L., Gao, J., Liu, A., 2009. Catalytic performance and characterization of Ni-doped HZSM-5 catalysts for selective trimerization of n-butene. Fuel Process. Technol. 90, 863–870.
Zheng, J., Cui, X., Yang, Q., Ren, Q., Yang, Y., Xing, H., 2018. Shaping of ultrahigh-loading MOF pellet with a strongly anti-tearing binder for gas separation and storage. Chem. Eng. J. 354, 1075–1082.
Zheng, X., Ren, S., Gai, Q., Liu, W., Dong, Q., 2021. Covalent-bond-enhanced photocatalytic hydrogen evolution of C_3N_4/CoP_x with L-cysteine molecule as bridging ligands. Appl. Surf. Sci. 569, 151025.
Zhou, N., Dai, L., Lyu, Y., Wang, Y., Li, H., Cobb, K., Chen, P., Lei, H., Ruan, R., 2022. A structured catalyst of ZSM-5/SiC foam for chemical recycling of waste plastics via catalytic pyrolysis. Chem. Eng. J. 440, 135836.